remote sensing

MDPI

Article

Maneuvering Extended Object Tracking with Modified Star-Convex Random Hypersurface Model Based on Minimum Cosine Distance

Lifan Sun [1,2], Jinjin Zhang [1], Haofang Yu [3], Zhumu Fu [1,*] and Zishu He [2]

1 School of Information Engineering, Henan University of Science and Technology, Luoyang 471023, China
2 School of Information and Communication Engineering, University of Electronic Science and Technology of China, Chengdu 611731, China
3 School of Automation, Nanjing University of Technology, Nanjing 210094, China
* Correspondence: fuzhumu@haust.edu.cn

Abstract: Maneuvering extended object tracking is a new research field due to the rapid development of modern sensor technology. Multiple measurements may be resolved from different unknown sources on an object by using a high-resolution radar. In this case, the object should be regarded as an extended one with object extension, e.g., its shape may be described by the star-convex random hypersurface model. This model is usually specified by a one-dimensional radial function. However, the divergence of the shape estimation and a high error of the kinematic state estimation are likely to occur when an extended object maneuvers. This is because the radial function may take a negative value after Fourier series expansion, which leads to unpredictable estimation results. Unfortunately, the model itself is unable to solve this problem via the subsequent iterations. In this paper, we proposed a modified shape estimation approach to track an extended object with a star-convex random hypersurface model based on minimum cosine distance. Both the extension state and kinematic state at the current time are reinitialized once the radial function takes a negative value. Moreover, a mathematical model was constructed by using the principle of minimum cosine distance, so as to obtain more reasonable weight distribution coefficients for the correction of the extension state. Simulation results in different scenarios demonstrated the effectiveness of the proposed tracking approach.

Keywords: maneuvering extended object tracking; random hypersurface model; star-convex shape; minimum cosine distance; radial function

Citation: Sun, L.; Zhang, J.; Yu, H.; Fu, Z.; He, Z. Maneuvering Extended Object Tracking with Modified Star-Convex Random Hypersurface Model Based on Minimum Cosine Distance. *Remote Sens.* **2022**, *14*, 4376. https://doi.org/10.3390/rs14174376

Academic Editors: Junjie Wu, Xiaolong Chen, Jibin Zheng and Bo Chen

Received: 26 July 2022
Accepted: 24 August 2022
Published: 3 September 2022

1. Introduction

This paper focuses on radar object tracking. As illustrated in Figure 1, the ground radar station first sends an electromagnetic wave to the object, and then the sensor receives measurement data from the object [1]. Finally, the object state is continuously estimated by developing a mathematical model and combining the filtering steps. In the traditional radar tracking algorithm, it is assumed that each time only a single point positional measurement of a target is available. With the fast development of high-resolution sensors, this assumption is no longer valid in current tracking scenarios because the received multiple measurements may originate from different unknown sources on an object. For example, a high-resolution radar can resolve individual features and kinematic measurements. In this case, the object should be considered as an extended one with spatial extension (i.e., size, shape and orientation) [2].

The task of extended object tracking can be summarized as a joint estimation of the kinematic state and extension state. There exists an inherent coupling relationship between shape and motion. On the one hand, obtaining an accurate kinematic state will naturally be conducive to the estimation of the shape since the orientation of the object is always aligned with its motion direction [3]. On the other hand, a description close to the true shape will help to capture the position of the object, so that the object can be accurately tracked. Overall, knowing the target's range extent is extremely useful for improving the precision and robustness of both shape and motion estimation [4]. As a result, modeling the spatial extension is a critical component of extended object tracking in order to jointly estimate shape extension and centroid kinematics.

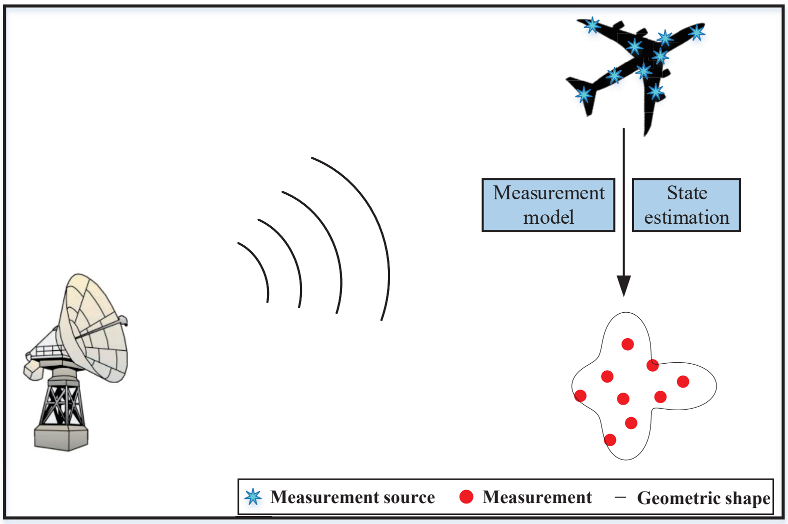

Figure 1. Status diagram of radar object tracking.

The existing morphological modeling methods of an extended object primarily include those based on random matrix (RM) [5–7] and the random hypersurface model [8,9]. They are then integrated into a filtering algorithm based on random finite set (RFS) [10–12], which can not only track the object accurately but also estimate its external contour shape at the same time. Koch first proposed the Random Matrix modeling method in [13]. It is, however, limited to objects whose shape can be simplified to an ellipse, and cannot describe more complex shapes. To describe the vehicles on the road, Granstrom et al. proposed a rectangular model. Using the measured data from the laser ranging sensor, this method estimated the target's size, shape and motion state [14]. Unfortunately, because more details on the shape cannot be ignored when the object is close to the sensor, some simple geometries (ellipse, rectangle, etc.) are insufficient to describe the shape. Then, Lan and Li proposed that multiple ellipses be combined to describe the shape of non elliptical objects or object groups [15]. In a nutshell, the Random Matrix-based methods are only appropriate for describing some basic shapes (circle, ellipse, rectangle, etc.). Although those shapes can reflect relevant information about orientation and extent, they are still insufficient for many extended object tracking scenarios.

To solve this problem, Baum proposed the random hypersurface model (RHM), which can describe not only elliptical but also more complex shapes such as star-convex [16,17]. A radial function can be used to describe the contour of the star-convex extended object. Its size represents the distance between each contour point and the orientation. As a nonlinear polar function, the radial function must be linearized, i.e., Fourier series expansion, and its coefficients reflect the detailed information of the shape [18]. However, there exists an inevitable defect. Once the radial function has a negative value in the linearization process, the phenomenon of shape divergence will occur. Moreover, the error cannot be corrected by the model itself, which will inevitably result in a sharp decline in estimation accuracy or even a tracking failure. Both [18,19] pointed out that the estimation result will be unpredictable if this constraint condition is not satisfied. Furthermore, ref. [19] improves the original star-convex model by taking nonlinear inequality constraints into account, in which a sampling constraint and a conservative constraint are discussed, respectively.

This method can effectively avoid the problem of shape divergence, but there is still room for further improvement of estimation accuracy. Nevertheless, to the best of our knowledge, there is no effective solution to overcome this defect. Hence, this paper analyzes the existing star-convex RHM and develops a modified shape estimation method to optimize the original model.

Since the shape and motion state of the object change continuously, the prior information and historical results can be effectively utilized to alleviate this inherent demerit. Specific solutions are as follows: In the linearization process, once the radial function has a negative value, the extension parameter and kinematic state can be reinitialized at current time. This should be accompanied by the filtering process. The specific reinitialization operation is to retain the kinematic state of the previous step. The extension parameters are replaced by the weighted values of those at the initial time and the last time. The weight here is adaptive based on the principle of minimum cosine distance. The basis for this operation can be attributed to the fact that the state of the last time actually already contains the information of all the previous times. Via numerical simulation experiments in three different scenarios, the proposed method was shown to possess superior performance.

The paper is organized as follows. In Section 2.1, the random hypersurface model and maneuver modeling for shape estimation of star-convex extended object are introduced. Additionally the shape divergence problem when the constraint conditions are not satisfied is analyzed simultaneously in Section 2.1. Section 2.2 presents the method proposed in this paper. The simulation experiments are conducted in Section 3 to prove the effectiveness and rationality of the proposed method. The next section summarizes and analyzes the simulation results. The last Section 5 provides the conclusion.

2. Materials and Methods

2.1. Problem Formulation

The task of extended object tracking can be attributed to the joint estimation of kinematic and extension states. Suppose that the state vector of the object at k is $\boldsymbol{x}_k = \left(\boldsymbol{x}_k^m, \boldsymbol{x}_k^e\right)^T$, where $\boldsymbol{x}_k^m$ and $\boldsymbol{x}_k^e$ denote the kinematic and extension state vector, respectively. The dynamic equation followed by the evolution of the object state is:

$$\begin{bmatrix} \boldsymbol{x}_{k+1}^m \\ \boldsymbol{x}_{k+1}^e \end{bmatrix} = \begin{bmatrix} \boldsymbol{F}_k^m & 0 \\ 0 & \boldsymbol{F}_k^e \end{bmatrix} \begin{bmatrix} \boldsymbol{x}_k^m \\ \boldsymbol{x}_k^e \end{bmatrix} + \begin{bmatrix} \boldsymbol{w}_k^m \\ \boldsymbol{w}_k^e \end{bmatrix}, k \in N \tag{1}$$

where $\boldsymbol{F}_k^m$ and $\boldsymbol{F}_k^e$ are the state transition matrix of the kinematic state and extension state, respectively. $\boldsymbol{w}_k^m \sim \mathcal{N}(0, Q_k^m)$ is an independent Gaussian process noise, $\boldsymbol{w}_k^e \sim \mathcal{N}(0, Q_k^e)$ also denotes a Gaussian independent process, and both them are independent of each other.

The kinematic state of the object is denoted by a random variable $\boldsymbol{x}_k^m = \left(x_k, v_{k(x)}, y_k, v_{k(y)}\right)^T$, where $(x_k, y_k)^T$ and $\left(v_{k(x)}, v_{k(y)}\right)^T$ represent the position and velocity of the centroid, respectively. The dynamic evolution equation of the above motion variables is

$$\mathbf{x}_{k+1}^m = \mathbf{F}_k^m \mathbf{x}_k^m + \mathbf{w}_k^m \tag{2}$$

Supposing that the extended object makes constant-turning motion with a rotation rate of ω, and the rotation angle within the same sampling time T is denoted as φ=ωT. Then, the corresponding state transition matrix $\mathbf{F}_k^m(\varphi)$ of the dynamic variable $\mathbf{x}_k^m$ is [20]

$$\mathbf{F}_k^m(\varphi) = \begin{bmatrix} 1 & \frac{\sin(\varphi)}{\omega} & 0 & -\frac{1-\cos(\varphi)}{\omega} \\ 0 & \cos(\varphi) & 0 & -\sin(\varphi) \\ 0 & \frac{1-\cos(\varphi)}{\omega} & 1 & \frac{\sin(\varphi)}{\omega} \\ 0 & \sin(\varphi) & 0 & \cos(\varphi) \end{bmatrix} \tag{3}$$

In the two-dimensional Cartesian coordinate system, if the object makes a constant-acceleration motion, then the kinematic state can be denoted by

$\boldsymbol{x}_k^m = \left(x_k, v_{k(x)}, a_{k(x)}, y_k, v_{k(y)}, a_{k(y)}\right)^T$, where a_x and a_y denotes the acceleration along the x-axis and y-axis directions, respectively. Additionally, the transition matrix of the corresponding kinematic state is [20]

$$\boldsymbol{F}_k^m(a_x, a_y) = \begin{bmatrix} 1 & T & \frac{T^2}{2} & 0 & 0 & 0 \\ 0 & 1 & T & 0 & 0 & 0 \\ 0 & 0 & 1 & 0 & 0 & 0 \\ 0 & 0 & 0 & 1 & T & \frac{T^2}{2} \\ 0 & 0 & 0 & 0 & 1 & T \\ 0 & 0 & 0 & 0 & 0 & 1 \end{bmatrix} \tag{4}$$

The extension state of the extended object is described by the random hypersurface model, which has an advantage over other morphological modeling methods, in that it can use more detailed information to describe some complex shapes [21]. For instance, the star-convex shape can more accurately approximate the true shape of the aircraft compared to other shapes (such as ellipse, see Figure 2 below). In other words, it can model a wide range of object shapes, including irregular shapes with complex geometry. As such, more detailed features can be captured. That is why we used the random hypersurface model to model the extension state of an extended object as a star-convex shape in this paper.

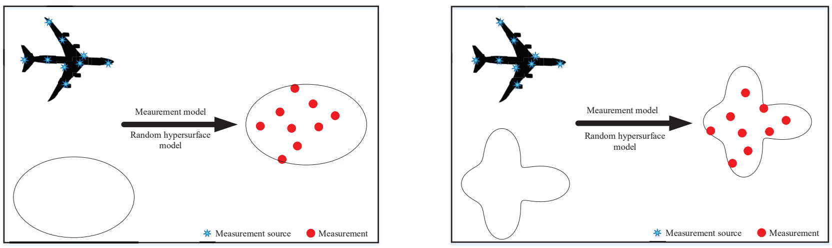

(**a**) (**b**)

Figure 2. Illustration of approximating an extended object with ellipse/star-convex. (**a**) Ellipse. (**b**) Star-convex.

2.1.1. Star-Convex Random Hypersurface Model

The contour of a star-convex object can be described by the radial function, and its size represents the distance between each contour point and center point of the object. As illustrated in Figure 3, φ represents the angle between the line from the center point x_k^c to the contour point, the X-axis, $r(\varphi)$ denotes the distance, and $\hat{s}_k \in [0,1]$ represents the scaling factor. The scaled object contour $\overline{S}(x_k)$ can be described as follows:

$$\overline{S}(x_k) = \{\hat{s}_k r(\varphi)\boldsymbol{e}(\varphi) + x_k^c | \varphi \in [0, 2\pi), \hat{s}_k \in [0,1]\} \tag{5}$$

$$\boldsymbol{e}(\varphi) = \begin{bmatrix} \cos(\varphi) \\ \sin(\varphi) \end{bmatrix} \tag{6}$$

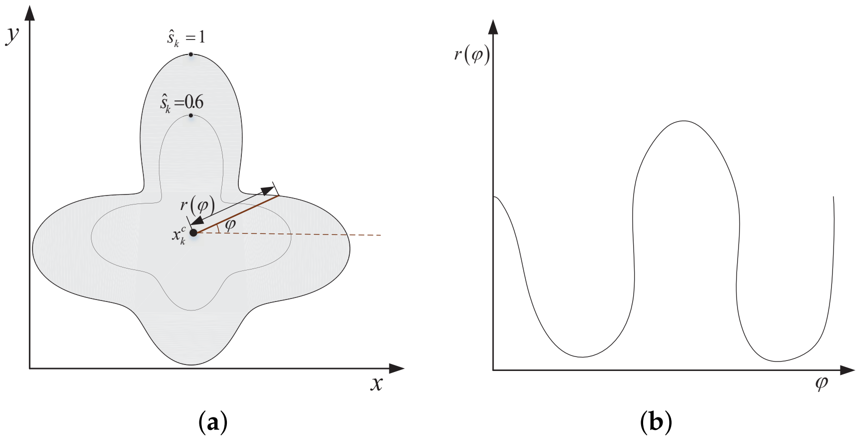

Figure 3. Representation of a star-convex shape using a radial function. (**a**) Star-convex extended object. (**b**) Radial function.

The radial function is then linearized, i.e., Fourier series expansion is applied, which can be formulated as follows:

$$r(\boldsymbol{B}_k, \varphi) = a_k^{(0)} + \sum_{j=1,\cdots,N^{\mathrm{F}}} \left(a_k^{(j)} \cos(j\varphi) + b_k^{(j)} \sin(j\varphi) \right) = \boldsymbol{R}(\varphi)\boldsymbol{B}_k \tag{7}$$

$$\boldsymbol{R}(\varphi) = \left[1, \cos(\varphi), \sin(\varphi), \ldots, \cos\left(N^{\mathrm{F}}\varphi\right), \sin\left(N^{\mathrm{F}}\varphi\right)\right] \tag{8}$$

$$\boldsymbol{B}_k = \left[a_k^{(0)}, a_k^{(1)}, b_k^{(1)}, \ldots, a_k^{\left(N^{\mathrm{F}}\right)}, b_k^{\left(N^{\mathrm{F}}\right)}\right]^{\mathrm{T}} \tag{9}$$

where N^{F} denotes the order of Fourier series expansion. In fact, the higher the order, the more detailed features can be captured. On the contrary, if the order is low, only rough features can be obtained, which will eventually result in the loss of information. Equation (9) illustrates the coefficients expanded by the Fourier series, which can reflect the shape information of the extended object. Therefore, the extension parameter vector $\boldsymbol{x}_k^e$ of the object can be represented by $\boldsymbol{B}_k$ as follows:

$$\boldsymbol{x}_k^e = \left[a_k^{(0)}, a_k^{(1)}, b_k^{(1)}, \ldots, a_k^{\left(N^{\mathrm{F}}\right)}, b_k^{\left(N^{\mathrm{F}}\right)}\right]^{\mathrm{T}} \tag{10}$$

In this paper, the extension parameter contains nine variables, i.e., $N_F = 4$. When using the RHM to estimate the extension state, the initial shape is generally modeled as a circle, then the measurement and filtering process are used to complete the subsequent iterative process. Assuming that the object moves according to the maneuvering status in Table 1, then a dynamic evolution process of the estimated shape can be shown in Figure 4. Here, the black and red boundaries represent the true shape and estimated results, respectively. Initially, the shape is generally modelled as a circle, and the estimated result becomes gradually close to the true shape with the subsequent step-by-step iterative process. From Figure 4, it can be easily noted that the estimated result gradually evolved from the initial circle to the star-convex shape.

Table 1. Maneuvering process.

Step	[1,20)	[20,40)	[40,60)	[60,80)	[80,100)
w(rad/s)	−5	−10	0	−5	−10

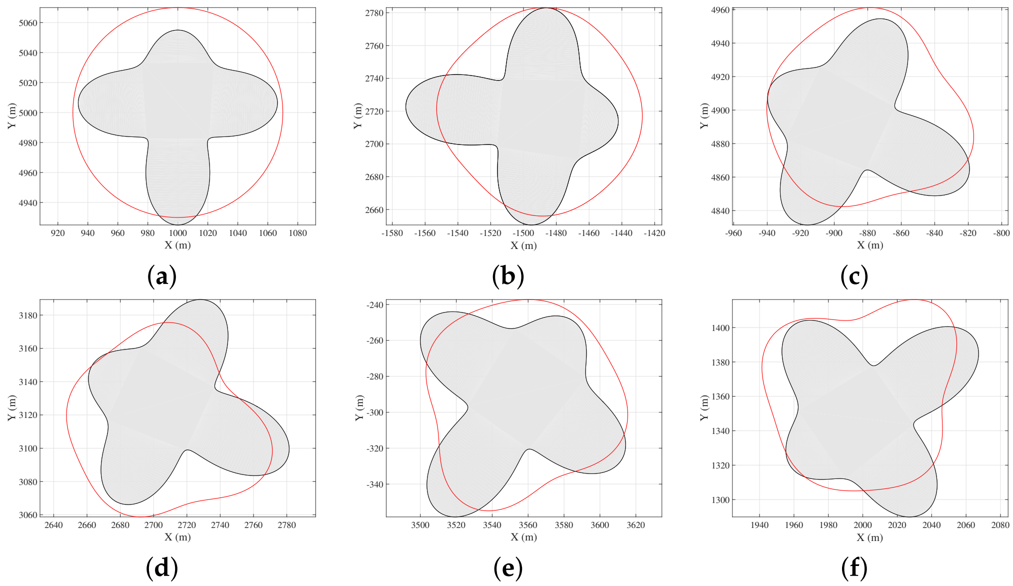

Figure 4. The whole iterative process of shape estimation for star-convex object. (**a**) Step-1. (**b**) Step-20. (**c**) Step-40. (**d**) Step-60. (**e**) Step-80. (**f**) Step-100.

There exists a close coupling relationship between the motion direction and orientation of the object during maneuvering. Especially in the scene of constant turning, the maneuver of the centroid and the rotation of the extended form occur simultaneously. Of course, if the object is treated as a point, the influence of maneuver on the shape does not need to be considered. Nevertheless, as for the extended object, this problem can no longer be ignored. Therefore, there is a pressing need to establish the maneuvering model of the extended object with a star-convex shape.

2.1.2. Maneuvering Modeling of Extended Object with Star-Convex Shape

The simulation test in this paper was mainly completed in the constant turning scene, so here only the evolution process of morphological variables during a turning maneuver is provided. On the one hand, $\mathbf{F}_k^e(\varphi)$ is closely related to the coefficient vector after the Fourier series expansion of the radial function. On the other hand, when the object rotates with an angle θ, the radial function also shifts by the same angle [22]. Therefore, in consideration of this property, the radial function after the rotation angle θ can be calculated according to the radial function before maneuver, that is

$$r\left(\mathbf{x}_{k+1}^{\mathrm{e}}, \phi\right) = r\left(\mathbf{x}_k^e, \phi - \theta\right) + \mathbf{w}_k^e \tag{11}$$

where ϕ defines the angle after rotation, $\mathbf{x}_{k+1}^{\mathrm{e}}$ represents the morphological variable obtained at $k+1$, and $\mathbf{w}_k^e$ represents the noise in the process of morphological variable transfer. The result of Fourier expansion can be expressed as

$$\begin{aligned} & a_{k+1}^{(0)} + \sum_{j=1,\cdots,N_{\mathrm{F}}} \left(a_{k+1}^{(j)} \cos(j\phi) + b_{k+1}^{(j)} \sin(j\phi)\right) = \\ & a_k^{(0)} + w_k^{(0)} + \sum_{j=1,\cdots,N_{\mathrm{F}}} \left(\left[a_k^{(j)} \cos(j\theta) - b_k^{(j)} \sin(j\theta)\right] \cos(j\phi) + w_k^{(2j-1)} + \right. \\ & \left. \left[a_k^{(j)} \sin(j\theta) + b_k^{(j)} \cos(j\theta)\right] \sin(j\phi) + w_k^{(2j)}\right) \end{aligned} \tag{12}$$

Then, it can be further collated to the following equations.

$$a_{k+1}^{(0)} = a_k^{(0)} + w_k^{(0)} \tag{13}$$

$$a_{k+1}^{(j)} = a_k^{(j)} \cos(j\theta) - b_k^{(j)} \sin(j\theta) + w_k^{(2j-1)} \tag{14}$$

$$b_{k+1}^{(j)} = a_k^{(j)} \sin(j\theta) + b_k^{(j)} \cos(j\theta) + w_k^{(2j)} \tag{15}$$

Therefore, the variables in the extension parameter vector x_{k+1}^{e} are denoted as follows.

$$\mathbf{x}_{k+1}^{\mathrm{e}} = \mathbf{F}_k^{e}(\theta)\mathbf{x}_k^{\mathrm{e}} + \mathbf{w}_k^{\mathrm{e}} \tag{16}$$

$$\mathbf{F}_k^{e}(\theta) = \begin{bmatrix} 1 & 0 & 0 & 0 & 0 & 0 & 0 & 0 & 0 \\ 0 & \cos\theta & -\sin\theta & 0 & 0 & 0 & 0 & 0 & 0 \\ 0 & \sin\theta & \cos\theta & 0 & 0 & 0 & 0 & 0 & 0 \\ 0 & 0 & 0 & \cos 2\theta & -\sin 2\theta & 0 & 0 & 0 & 0 \\ 0 & 0 & 0 & \sin 2\theta & \cos 2\theta & 0 & 0 & 0 & 0 \\ 0 & 0 & 0 & 0 & 0 & \cos 3\theta & -\sin 3\theta & 0 & 0 \\ 0 & 0 & 0 & 0 & 0 & \sin 3\theta & \cos 3\theta & 0 & 0 \\ 0 & 0 & 0 & 0 & 0 & 0 & 0 & \cos 4\theta & -\sin 4\theta \\ 0 & 0 & 0 & 0 & 0 & 0 & 0 & \sin 4\theta & \cos 4\theta \end{bmatrix} \tag{17}$$

Following this, the dynamic evolution equation of morphological variables in the turning maneuver scene can be obtained as illustrated in Equation (16), where $\mathbf{F}_k^{e}$ is the state transition matrix, which has the form expressed in Equation (17). Taking Equations (3) and (17) into Equation (1), the dynamic evolution equation of a star-convex extended object under a turning scene can be obtained.

$$x_{k+1} = \begin{bmatrix} F_{k,m}(\phi) & 0 \\ 0 & F_{k,e}(\phi) \end{bmatrix} x_k + w_k, k \in N \tag{18}$$

The above model can uniformly describe the left-turning and right-turning motion of a star-convex extended object under different rotation rates. When the rotation rate is 0, the above equation degenerates into a dynamic equation of uniform linear motion [22]. At this time, the transfer matrices of the kinematic and extension state are as follows.

$$\mathbf{F}_k^{m}(\theta) = \begin{bmatrix} 1 & T & 0 & 0 \\ 0 & 1 & 0 & 0 \\ 0 & 0 & 1 & T \\ 0 & 0 & 0 & 1 \end{bmatrix} \tag{19}$$

$$\mathbf{F}_k^{e}(\theta) = \mathrm{diag}(1, 1, 1, \ldots, 1, 1) \tag{20}$$

However, there still exists room for improvement in the above morphological modeling process proposed in Sections 2.1.1 and 2.1.2. A defect of the radial function is that there exists an implicit non-negative constraint, i.e., the distance from the center to the boundary point given an angle θ must always be positive [18]. If this important constraint is not taken into account, the estimation results will be unpredictable, which can be clearly confirmed by the example in Figure 5. Therefore, the approximation of radial function must always be positive to ensure that it conforms to the fundamental definition of geometry, especially the star-convex shape. Nevertheless, since the radial function is a nonlinear function, only an approximate value by performing Fourier expansion during the linearization process can be obtained. It is obvious that such an operation cannot guarantee that the approximated value is always nonnegative.

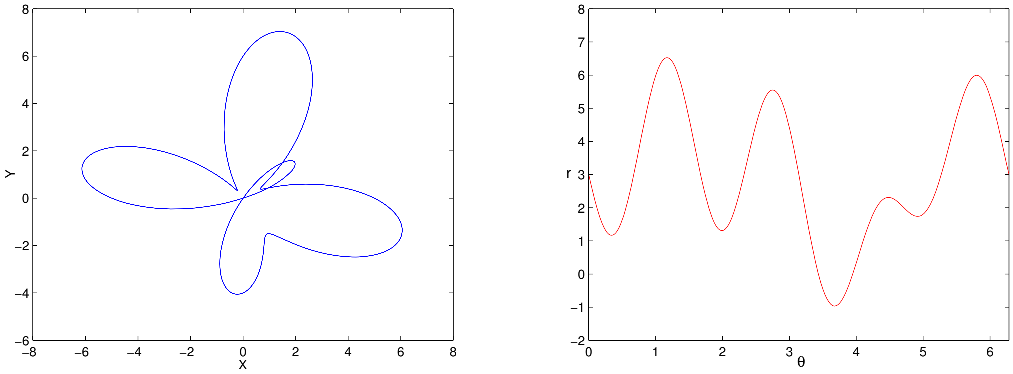

(a) (b)

Figure 5. Estimation results without considering the constraint. (**a**) Estimated shape. (**b**) Approximation of the radial function.

Furthermore, due to the inherent coupling relationship between shape and motion, the estimation accuracy of the kinematic state will also be significantly reduced, leading to tracking failure. As illustrated in Figure 6, the estimation results of shape at some steps obviously deviated from the truth, leading to a huge estimation error. Moreover, the model itself is unable to correct this error through the subsequent iterative process. In general, it is sufficient to conclude that tracking fails due to such poor performance. Therefore, there is an urgent need to propose a novel method to avoid tracking failure once the radial function acquires a negative value.

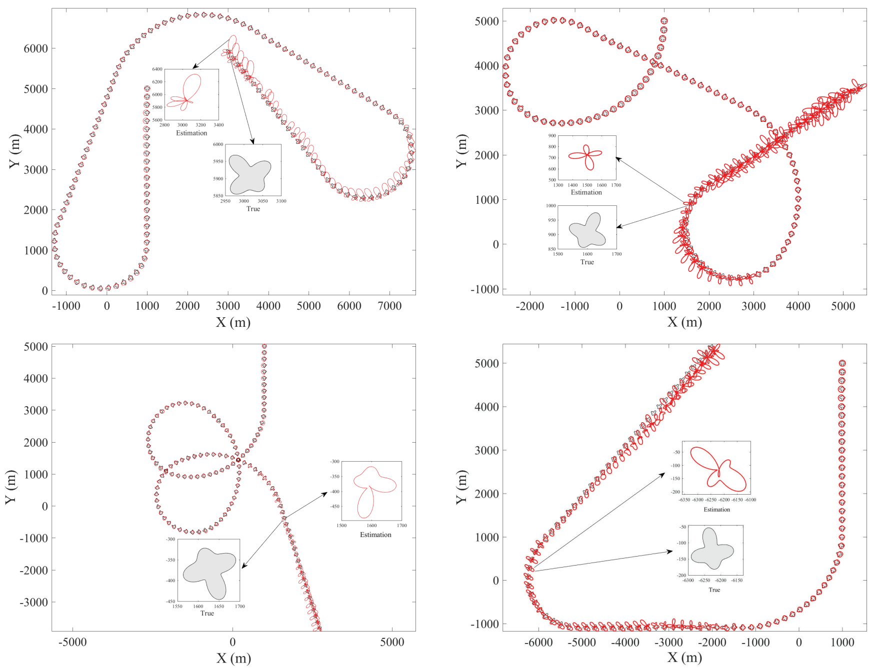

Figure 6. Shape divergence in some typical scenarios.

Considering that the motion and shape of the object vary continuously between uninterrupted sampling times, i.e., there exists consistency and continuity, the parameters of the previous time must contain some information about the current time. Therefore, we can make full use of the information carried in the historical results to improve or avoid the serious consequences caused by this situation.

2.2. Proposed Approach

According to the previous analysis of the causes of tracking failure, the root of the problem can be found in the initialization process. Naturally, adding a novel reinitialization process to the original model to avoid tracking failure when the radial function acquires a negative value is considered in this paper. The process of reinitialization can be summarized as follows: Initially, the value of the radial function after filtering at k is judged. If it is positive, continue with the next iteration. However, if it is negative, a novel reinitialization step needs to be executed, i.e., both the kinematic state $\boldsymbol{x}_k^m$ and extension parameter $\boldsymbol{x}_k^e$ are reinitialized. Eventually, the multi-model estimation process [23] is performed again. The following are the specific steps of parameter reinitialization:

Assuming that $\boldsymbol{x}_o^e$ denotes the shape information at the initial time, $\hat{\boldsymbol{x}}_{k-1}^m$ and $\hat{\boldsymbol{x}}_{k-1}^e$ are the kinematic state and extension parameter vectors at $k-1$, respectively. Compared with the historical information of earlier steps, the state (both kinematic and extension) at $k-1$ is certainly closer to the current state. Therefore, the kinematic state (including position, velocity, etc.) at $k-1$ can be used to reinitialize $\boldsymbol{x}_k^m$. However, since the decline of estimation accuracy is fundamentally caused by shape divergence, if only the extension parameter at $k-1$ is utilized for the reinitialization of $\boldsymbol{x}_k^e$, it will inevitably lead to tracking failure again for the same reason. The shape at the initial time is assumed to be a circle, which belongs to a kind of convex polygon, and the radial function in the polar coordinate system must always be positive. Nevertheless, all the shape information obtained before k will be lost if only the shape at the initial time is used to reinitialize the extension parameter. This leads to a limited correction capability. Therefore, in this paper, the shape information of initial time and historical time is fused to reinitialize the extension parameter.

Since the extension parameters of the first d steps carry the historical information of the shape, weighting of the extension parameters at the initial step and the first d steps is considered to obtain $\tilde{\boldsymbol{x}}_k^e$. $\tilde{\boldsymbol{x}}_k^e$ denotes the extension parameter after reinitialization, and the size of d is determined by traversing the value of d in this paper. Taking the second one in Figure 6 as the maneuvering scenario, simulation tests were conducted for different d values from 1 to 6. Under each hypothesis, a total of 100 simulation tests were carried out. Figure 7 and Table 2 depict the correction ability corresponding to different d, where Hausdorff distance [24] and root-mean-square error (RMSE) are used to evaluate the shape and motion correction ability of different d, respectively. The smaller the value, the better the correction capability.

As shown in Figure 7 and Table 2, a conclusion can be easily drawn in that the performance is the best for $d = 1$. This suggests that a better correction ability can be achieved only by using the shape information at $k-1$ and the initial time. This is primarily because the state of the object is continuously changing, so the shape at $k-1$ (i.e., $d = 1$) actually carries the historical information of an earlier time. If $d > 1$ (i.e., all the information of the previous d steps are weighted), and by reusing some historical information, the operation will not improve the correction ability but increase the computational burden. Therefore, we decided to weight $\boldsymbol{x}_o^e$ and $\hat{\boldsymbol{x}}_{k-1}^e$ to obtain the extension parameter $\tilde{\boldsymbol{x}}_k^e$ after reinitialization.

Table 2. The correction ability corresponding to different d.

	Hausdorff Distance (d_H/m)	Position RMSE (m)	Velocity RMSE (m/s)
$d = 1$	347.398	21.024	12.679
$d = 2$	352.467	30.800	23.377
$d = 3$	354.406	29.167	20.527
$d = 4$	352.814	24.228	15.249
$d = 5$	350.161	23.259	16.296
$d = 6$	354.790	34.242	25.129

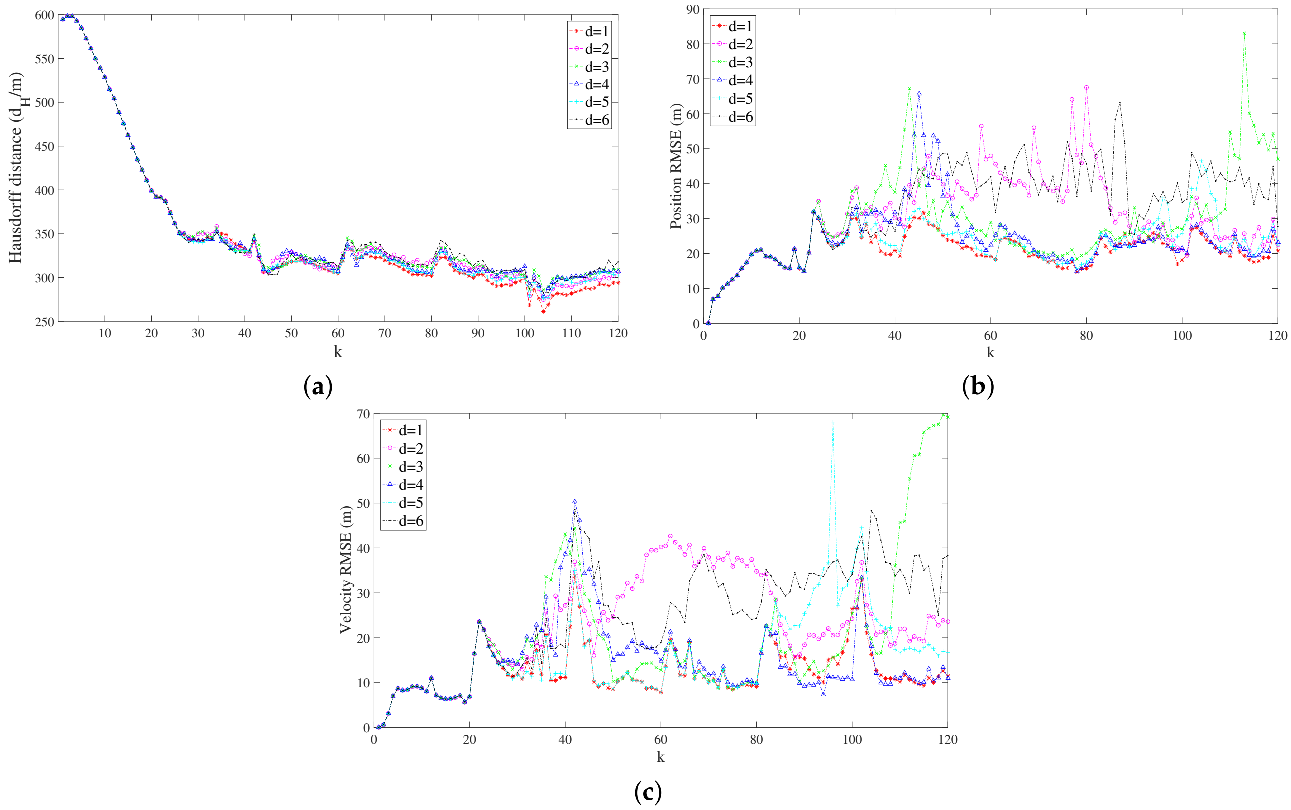

Figure 7. The correction ability with different values of d. (**a**) Hausdorff distance. (**b**) RMSE of position. (**c**) RMSE of velocity.

Meanwhile, the determination of weight here is still a crucial yet difficult problem. If each weight distribution coefficient is artificially specified, a certain degree of subjective randomness is inevitably introduced. Moreover, the authority and reliability of each distribution cannot be guaranteed owing to the lack of experience. In general, the differences between the weighted extension parameter vector $\tilde{x}_k^e$ and the two before combination are expected to be small. As a result, some fuzzy decision-making problems typically employ objective methods to establish a planning model for the determination of attribute weights [25,26]. For instance, when using the combined weighting method to evaluate the system performance, the principle of minimum relative entropy is skillfully applied to determine the distribution coefficients of subjective and objective weights [27].

The difference between two random distributions is measured asymmetrically using relative entropy, also known as Kullback–Leibler divergence [28]. Assuming that $P(x)$ and $Q(x)$ are two probability distributions for a random variable x, the relative entropy in the case of discrete and continuous random variables can be defined as follows, respectively [29].

$$KL(P \parallel Q) = \sum P(x) \ln \frac{P(x)}{Q(x)}, KL(P \parallel Q) = \int P(x) \ln \frac{P(x)}{Q(x)} dx \tag{21}$$

If the two probability distributions are the same, their relative entropy is zero. When the difference between the two probability distributions increases, their relative entropy will also increase. The following is an equation used to calculate weight with the principle of minimum relative entropy:

$$\begin{cases} \min Q(p,q) = \sum\limits_{j=1}^{N} \tilde{x}_k^e \ln\left(\frac{\tilde{x}_k^e}{\hat{x}_{k-1}^e}\right) + \sum\limits_{j=1}^{N} \tilde{x}_k^e \ln\left(\frac{\tilde{x}_k^e}{x_o^e}\right) \\ p + q = 1, \tilde{x}_k^e = p * \hat{x}_{k-1}^e + q * x_o^e \end{cases} \tag{22}$$

where N indicates the number of variables in the extension parameter vector. x_o^e and $\hat{x}_{k-1}^e$ are the extension parameters at the initial time and $k-1$, p and q denote their weight distribution coefficients, respectively.

However, the logarithmic function's argument must be positive, i.e., the corresponding weighted variables in x_o^e and $\hat{x}_{k-1}^e$ must have the same sign, which obviously cannot be satisfied here. Therefore, the principle of minimum relative entropy is ineffective in determining the weight distribution coefficient in this paper. It is a blessing that it can be roughly replaced by another scale criterion for measuring vector difference. Cosine distance, also known as cosine similarity, can be used to evaluate the similarity of two vectors by calculating the cosine value of the angle between them [30]. Additionally, the difference is proportional to the cosine distance. As a result, the minimum cosine distance can be used in this paper to construct the mathematical model and calculate a more reasonable weight distribution coefficient [31]. The process can be formulated as follows:

$$\begin{cases} \min Q(p,q) = \sum_{j=1}^{N} dist\left(\tilde{x}_k^e, \hat{x}_{k-1}^e\right) + \sum_{j=1}^{N} dist\left(\tilde{x}_k^e, x_o^e\right) \\ p+q=1, \tilde{x}_k^e = p * \hat{x}_{k-1}^e + q * x_o^e \end{cases} \tag{23}$$

$$dist\left(\tilde{x}_k^e, \hat{x}_{k-1}^e\right) = 1 - \cos\left(\tilde{x}_k^e, \hat{x}_{k-1}^e\right) = \frac{\|\tilde{x}_k^e\|_2 \|\hat{x}_{k-1}^e\|_2 - \tilde{x}_k^e \cdot \hat{x}_{k-1}^e}{\|\tilde{x}_k^e\|_2 \|\hat{x}_{k-1}^e\|_2} \tag{24}$$

$$dist\left(\tilde{x}_k^e, x_o^e\right) = 1 - \cos\left(\tilde{x}_k^e, x_o^e\right) = \frac{\|\tilde{x}_k^e\|_2 \|x_o^e\|_2 - \tilde{x}_k^e \cdot x_o^e}{\|\tilde{x}_k^e\|_2 \|x_o^e\|_2} \tag{25}$$

Figure 8 illustrates an example of obtaining adaptive weights p and q by using the minimum cosine distance in one optimization process, where the x-axis represents the number of variables included in the extension parameter vector, and the y-axis represents the values corresponding to each variable. Each time the reinitialization step is performed, the dynamic adaptive p and q values will be obtained according to the principle of minimum cosine distance, so as to make the weight distribution more reasonable. Table 3 lists the complete calculation process of the modified star-convex random hypersurface model proposed above.

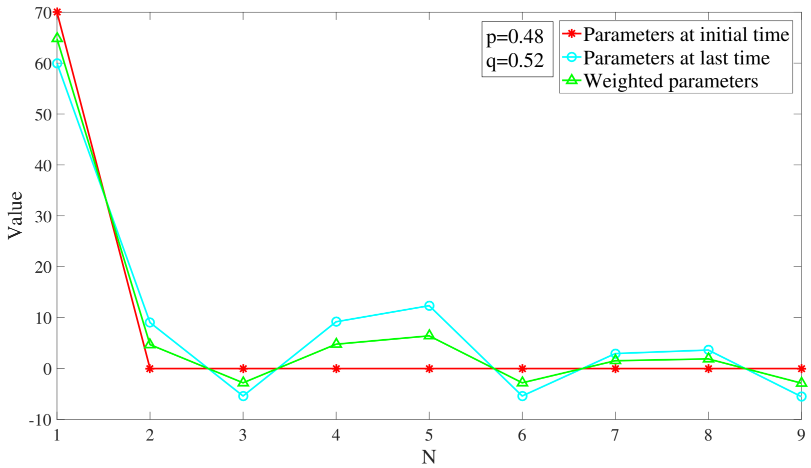

Figure 8. An example of using the minimum cosine distance to obtain adaptive weights.

Table 3. Pseudo codes of the proposed Method.

For $k = 1$

The scaled object contour can be described as

$\bar{S}(x_k) = \left\{ \hat{s}_k r(\varphi) e(\varphi) + x_k^c | \varphi \in [0, 2\pi), \hat{s}_k \in [0, 1] \right\}$

where $e(\varphi) = [\cos(\varphi), \sin(\varphi)]^T$.

Then, perform step ①.

① **Linearization process**

$$r(\varphi) = a_k^{(0)} + \sum_{j=1,\cdots,N^F} \left(a_k^{(j)} \cos(j\varphi) + b_k^{(j)} \sin(j\varphi) \right) = a_k^{(0)} + a_k^{(1)} \cos(\varphi) + b_k^{(1)} \sin(\varphi) + \cdots + a_k^{(N_F)} \cos(\varphi) + b_k^{(N_F)} \sin(\varphi)$$

If $r(\varphi) \geq 0$

$k = k + 1$, proceed to the next iteration.

Else

Perform step ②.

End if.

② **Reinitialization process**

$\tilde{\boldsymbol{x}}_k^m = \hat{\boldsymbol{x}}_{k-1}^m, \tilde{\boldsymbol{x}}_k^e = p * \boldsymbol{x}_o^e + q * \hat{\boldsymbol{x}}_{k-1}^e$.

where $\tilde{\boldsymbol{x}}_k^m$, $\tilde{\boldsymbol{x}}_k^e$ represent the kinematic and extension state after reinitialization.

p and q can realize adaptation through the following equations:

$$\min Q(p, q) = \sum_{j=1}^{N_F} dist\left(\tilde{\boldsymbol{x}}_k^e, \hat{\boldsymbol{x}}_{k-1}^e\right) + \sum_{j=1}^{N_F} dist\left(\tilde{\boldsymbol{x}}_k^e, \boldsymbol{x}_o^e\right)$$

$$p + q = 1, \tilde{\boldsymbol{x}}_k^e = p * \hat{\boldsymbol{x}}_{k-1}^e + q * \boldsymbol{x}_o^e$$

$$dist\left(\tilde{\boldsymbol{x}}_k^e, \hat{\boldsymbol{x}}_{k-1}^e\right) = 1 - \cos\left(\tilde{\boldsymbol{x}}_k^e, \hat{\boldsymbol{x}}_{k-1}^e\right) = \frac{\|\tilde{\boldsymbol{x}}_k^e\|_2 \|\hat{\boldsymbol{x}}_{k-1}^e\|_2 - \tilde{\boldsymbol{x}}_k^e \cdot \hat{\boldsymbol{x}}_{k-1}^e}{\|\tilde{\boldsymbol{x}}_k^e\|_2 \|\hat{\boldsymbol{x}}_{k-1}^e\|_2}$$

$$dist\left(\tilde{\boldsymbol{x}}_k^e, \boldsymbol{x}_o^e\right) = 1 - \cos\left(\tilde{\boldsymbol{x}}_k^e, \boldsymbol{x}_o^e\right) = \frac{\|\tilde{\boldsymbol{x}}_k^e\|_2 \|\boldsymbol{x}_o^e\|_2 - \tilde{\boldsymbol{x}}_k^e \cdot \boldsymbol{x}_o^e}{\|\tilde{\boldsymbol{x}}_k^e\|_2 \|\boldsymbol{x}_o^e\|_2}.$$

End for.

3. Results of Numerical Experiments

To prove the rationality and validity of the proposed method, the single maneuvering extended object was considered as the tracking target, and simulation experiments for two deterministic scenarios (DS1 and DS2) and one random scenario (RS) were performed, respectively. It should be noted that the paper primarily focused on improving the shape estimation method of star-convex RHM, so as to reduce the estimation error and eliminate the tracking failure caused by a negative value of the radial function, in which clutter and missed detection are not involved.

3.1. DS1

The simulation was carried out under the framework of Constant Velocity (CV) and Constant Turn (CT) models, in which both structure and parameter were altered. Table 4 details the maneuvering process of the object.

Table 4. Maneuvering process in DS1.

Step	[0,20)	[20,40)	[40,60)	[60,80)	[80,100)	[100,120]
w(rad/s)	−5	−10	0	−5	−10	0

The parameters of the initial value, state transition matrix and observation matrix used in the simulation process are set as follows:

$$\boldsymbol{x}_o^m = [1000 \text{ m}, 0 \text{ m/s}, 5000 \text{ m}, -200 \text{ m/s}] \tag{26}$$

$$\boldsymbol{x}_o^e = [70, 0, 0, 0, 0, 0, 0, 0, 0,] \tag{27}$$

$$z_k^j = \boldsymbol{H}_k^j x_k^j + v_k^j \tag{28}$$

where $\mathbf{x}_0^m$ and $\mathbf{x}_0^e$ are the initial kinematic and extension state, respectively. z_k^j denotes the jth two-dimensional measurement, v_k^j denotes the observation noise, and x_k^j in the turning scenario is $x_k^j = \left(x_k, v_{k(x)}, y_k, v_{k(y)}\right)^T$. Therefore, the observation matrix $\boldsymbol{H}_k^j$ in this simulation scenario can be set as follows:

$$\boldsymbol{H}_k^j = \begin{bmatrix} 1 & 0 & 0 & 0 \\ 0 & 0 & 1 & 0 \end{bmatrix} \tag{29}$$

In the above-mentioned simulation scenario, the traditional star-convex RHM was compared with the modified star-convex RHM proposed in this paper. Furthermore, to demonstrate the impact of weight on performance, the estimated results of using fixed weight and adaptive weight obtained by using minimum cosine distance are also compared. Figure 9, Tables 5 and 6 provide the performance comparisons of the three algorithms, in which the estimation accuracy of extension and kinematic state are evaluated using Hausdorff distance and RMSE, respectively. The smaller the values, the higher the estimation accuracy.

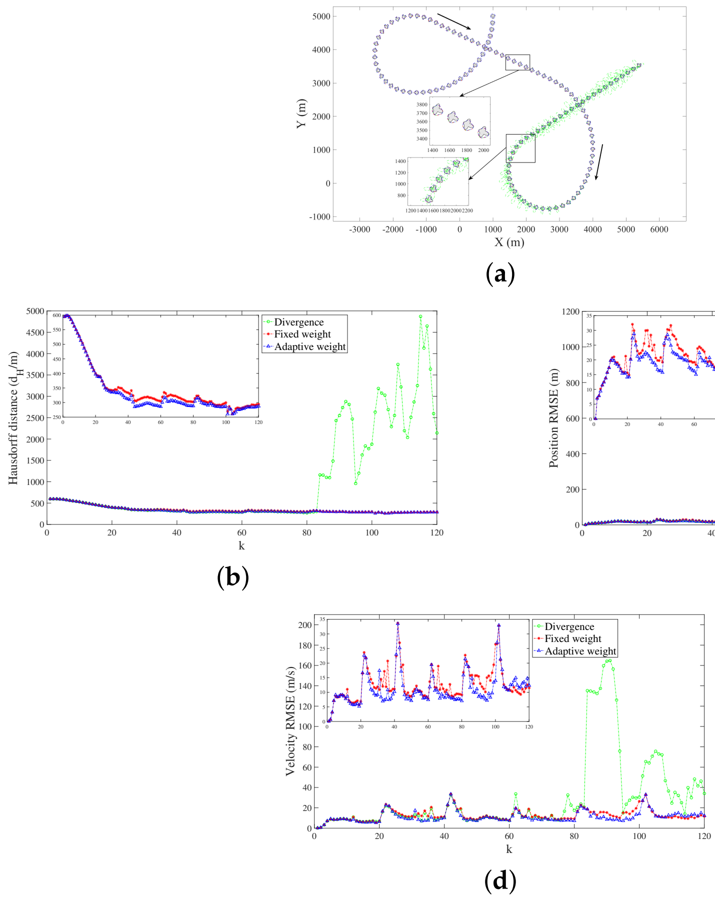

Figure 9. The performance comparisons of the three algorithms in DS1. (**a**) Trajectory. (**b**) Hausdorff distance. (**c**) RMSE of position. (**d**) RMSE of velocity.

Table 5. Performance comparisons of the three algorithms in DS1.

	Hausdorff Distance (d_H/m)	Position RMSE (m)	Velocity RMSE (m/s)
Divergence	1019.383	134.890	30.077
Fixed weight	347.398	21.024	12.679
Adaptive weight	337.000	19.051	11.110

Table 6. Computational burden of the three algorithms in DS1.

	Divergence	**Fixed Weight**	**Adaptive Weight**
Time (s)	1.000	1.049	1.046

According to the object trajectory in Figure 9a, the shape estimated by the original tracking algorithm had serious divergence from step 80. This suggests that the estimation results deviated from the true shape. Through the analysis of a large number of experimental data, it can be inferred that this situation was caused by the negative value of the radial function. Besides, from the subsequent tracking results of the original algorithm, a conclusion can be drawn that such an error cannot be repaired by the star-convex RHM itself. Therefore, after step 80, the original algorithm actually cannot complete the entire tracking process.

In reality, an inherent coupling relationship exists between the motion and the shape during the process of extended object tracking. For instance, the orientation of the object is always consistent with the moving direction of its centroid. Undoubtedly, the performance of both can benefit from the relationship, e.g., an accurate position is helpful to capture the object, and a description closer to the true shape is also conducive to the continuous tracking of the object. However, this relationship can also bring undesirable consequences. It can be observed from Figure 9c,d that there are significant errors in position and velocity due to shape divergence, especially in the estimation of centroid position, which directly leads to a tracking failure.

By using a reinitialization process, the algorithm proposed in this paper effectively solves this problem. Once the radial function is negative, the proposed algorithm can fully utilize the prior information and historical results to reinitialize the kinematic state and extension parameter, so as to effectively avoid the occurrence of tracking failure. Moreover, the proposed algorithm uses the minimum cosine distance to obtain more reasonable weight distribution coefficients and realize the weight adaptation. In this simulation process, the consequences of using fixed weight and adaptive weight are presented, respectively. The date in Tables 5 and 6 are sufficient to prove that using adaptive weight can achieve a more powerful correction of tracking results while marginally increasing the level of calculation.

3.2. DS2

To further validate the applicability and effectiveness of the proposed method in various tracking scenarios, simulation experiments were carried out in another typical turning scenario (DS2). The maneuvering process of the object is provided in Table 7. The settings of parameters such as initial value and transition matrix are consistent with those in DS1.

Table 7. Maneuvering process in DS2.

Step	**[0,20)**	**[20,40)**	**[40,60)**	**[60,80)**	**[80,100)**	**[100,120)**	**[120,140]**
w(rad/s)	0	-10	0	-5	0	-10	0

Similarly, the simulation results of the original star-convex RHM algorithm and the proposed algorithm (using fixed weight and adaptive weight, respectively) were compared. Figure 10, Tables 8 and 9 depict the performance comparison results of the three algorithms. To evaluate the estimation accuracy of extension and kinematic state, Hausdorff distance and RMSE were used, respectively.

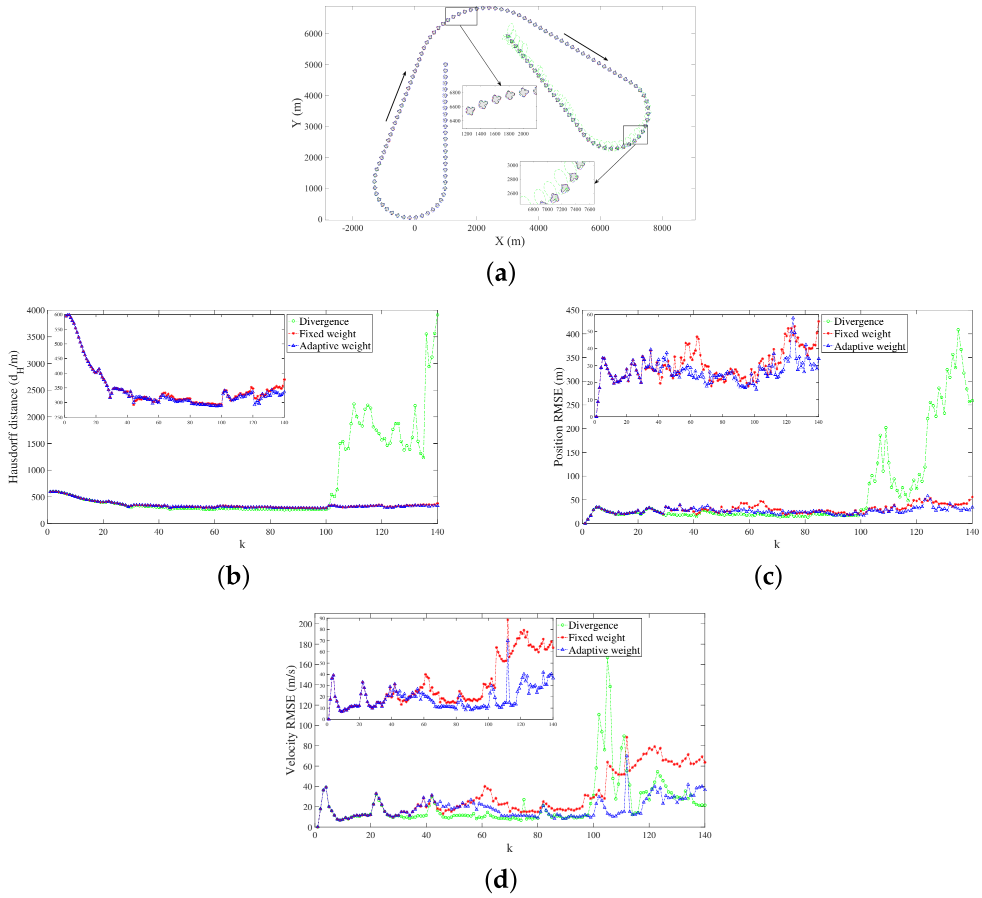

Figure 10. The performance comparisons of the three algorithms in DS2. (**a**) Trajectory. (**b**) Hausdorff distance. (**c**) RMSE of position. (**d**) RMSE of velocity.

Table 8. Performance comparisons of the three algorithms in DS2.

	Hausdorff Distance (d_H/m)	Position RMSE (m)	Velocity RMSE (m/s)
Divergence	749.464	64.666	22.318
Fixed weight	350.018	30.311	31.423
Adaptive weight	345.341	26.611	18.793

Table 9. Computational burden of the three algorithms in DS2.

	Divergence	Fixed Weight	Adaptive Weight
Time (s)	1.000	1.030	1.040

As demonstrated in Figure 10, when the program reaches 100 simulation steps, the shape divergence of the original algorithm occurs. Due to the inherent coupling relationship between shape and motion, the estimation results of the kinematic state are also affected, leading to a sudden increase in the corresponding RMSE of position and velocity. The error cannot be recovered by the model itself, and the shape estimation result after 100 simulation steps deviates from the true shape of the object.

Since the reinitialization method proposed in this paper was used for tracking, the estimation error reduced significantly, and the occurrence of tracking failure was effectively avoided. Furthermore, the proposed algorithm using adaptive weight can perform better when allocating the weights of extension parameters at the initial time and $k-1$. In particular, among the average error values of the three algorithms in Table 7, the average velocity error when using fixed weight is even larger than that of the original algorithm in some cases. The reasons include the following two aspects: on the one hand, the shape divergence makes a larger impact on the estimation accuracy of the position, so the velocity error is relatively small. On the other hand, the use of fixed weight actually introduces unnecessary prior information to a certain extent, leading to the uncertainty of the estimation results. In other words, once the fixed weight is assigned, the influence of human factors on the estimation results is introduced, increasing a degree of subjective randomness.

Overall, it can be concluded that the reinitialization method using adaptive weight proposed in this paper possesses superior performance when the radial function acquires a negative value, which can significantly reduce the tracking error so as to avoid tracking failure.

3.3. RS

To provide a fair performance comparison result, the experiment was carried out in a random scenario (RS). The program executes 100 simulation steps each time and randomly generates eight true motion states, in which both the time of duration τ_t and the corresponding turning rate w_k are random. The residence time τ_t of state $w = w_k$ is a random number that satisfies $\sum_{t=1}^{8} \tau_t = 100$. w_k represents a binomial distribution with mean $\bar{w}$ and variance ν^2. In this scenario, the sampling time is 1 s, and other relevant parameters are set as follows:

$$\bar{w} = 0, \nu^2 = 10 \tag{30}$$

During the entire maneuvering process, the object keeps turning at a constant velocity, and the turning rate changes eight times. This can be considered as a strong maneuvering process. Figure 11, Tables 10 and 11 demonstrate the performance comparison results of the three algorithms.

Table 10. Performance comparisons of the three algorithms in RS.

	Hausdorff Distance (d_H/m)	Position RMSE (m)	Velocity RMSE (m/s)
Divergence	465.977	123.770	23.451
Fixed weight	329.154	22.494	18.765
Adaptive weight	325.364	20.495	12.305

Table 11. Computational burden of the three algorithms in RS.

	Divergence	Fixed Weight	Adaptive Weight
Time (s)	1.000	1.056	1.059

In this simulation scenario, a total of 200 Monte Carlo simulation experiments were carried out with a random true trajectory generated each time. One of the trajectories is shown in Figure 11a. According to Figure 11a, when the program runs to step 70, the shape estimated by the original algorithm begins to diverge, resulting in a sudden increase in the

RMSE of the corresponding position and speed simultaneously. Combined with the Hausdorff distance of the three algorithms in Figure 11b, it can be observed that the proposed algorithm eliminates the shape divergence by using the proposed reinitialization method.

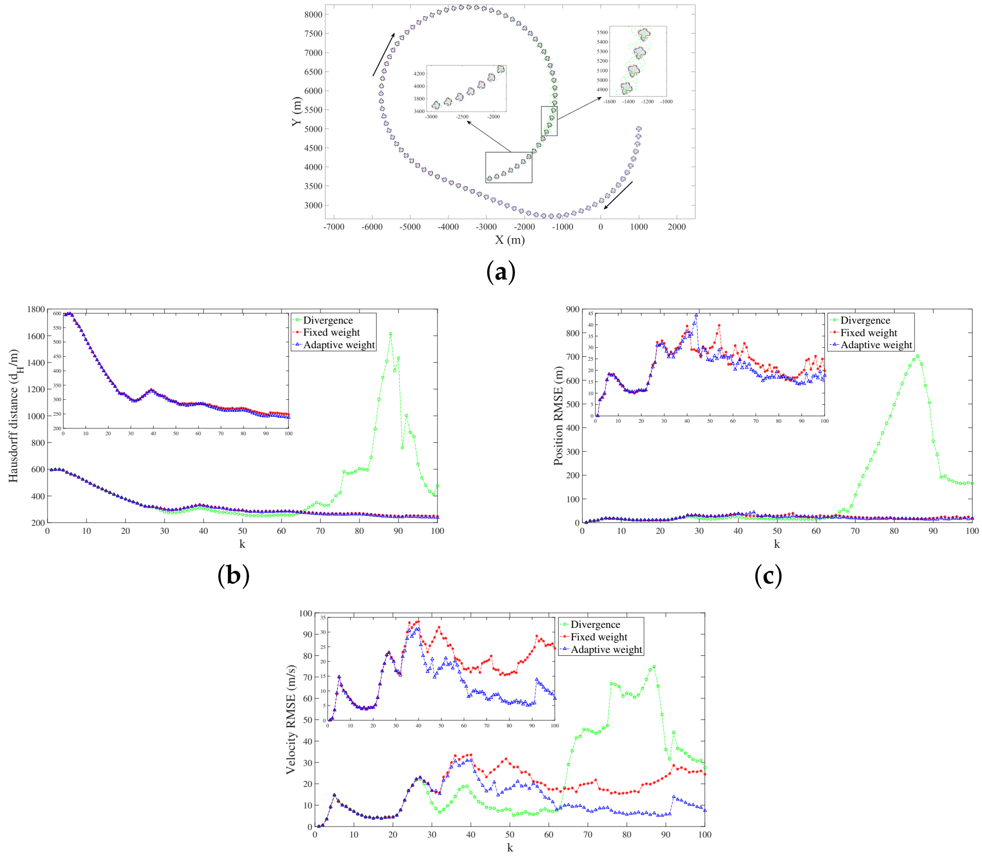

(a) (b) (c) (d)

Figure 11. The performance comparisons of the three algorithms in RS. (**a**) Trajectory. (**b**) Hausdorff distance. (**c**) RMSE of position. (**d**) RMSE of velocity.

Figure 11c,d illustrates the average error values of position and velocity in 200 Monte Carlo experiments, respectively. It is not difficult to find that the reinitialization method proposed in this paper can effectively reduce the tracking error compared with the original algorithm whether using fixed weight or adaptive weight. However, based on the analysis of values in Table 10, it is obvious that improved performance can be obtained when using the minimum cosine distance principle for weight adaptation. This is because of the automatic adjustment of the weight according to the initial and historical extension parameters when the reinitialization step is executed. In this random scenario, the performance comparison results of the three algorithms are more obvious than in the other two deterministic scenarios (DS1 and DS2), confirming the superiority of the algorithm proposed in this paper.

4. Discussion

According to the simulation results in Chapter 3, the algorithm proposed in this paper outperformed the competition in three maneuvering scenarios. The proposed algorithm, in particular, effectively solved the problem of shape divergence and greatly improved estimation accuracy. The reasons can be summarized as follows:

- A novel reinitialization step was added to the original model, which can effectively avoid the occurrence of tracking failure when the radial function acquires a negative value;

- When the extension parameter is reinitialized, the initial information and historical results are skillfully weighted, and the adaptive weight distribution coefficients are realized using the principle of minimum cosine distance.

This simulation experiments primarily focused on the tracking problem of a single maneuvering extended object; however, it is hoped that the proposed algorithm will be applicable to multi-object tracking in subsequent research.

5. Conclusions

In this paper, to solve the problem of tracking failure caused by the negative value of a radial function, a modified star-convex random hypersurface model was proposed. Once a negative value is detected, the initial extension parameter and historical results are fully utilized for reinitialization, and the principle of minimum cosine distance is used to obtain more reasonable weight distribution coefficients. Numerical simulation experiments were carried out in two typical deterministic scenarios (DS1 and DS2) and one random scenario (RS). It can be inferred from the experimental results that the proposed method can significantly improve the estimation accuracy of the original algorithm when the radial function has a negative value, so as to effectively avoid the tracking failure.

Author Contributions: L.S. and J.Z. conceived of the idea and developed the proposed approaches. H.Y. advised the research and helped edit the paper. Z.F. and Z.H. improved the quality of the manuscript and the completed revision. All authors have read and agreed to the published version of the manuscript.

Funding: The research was funded by the National Thirteen-Five Equipment Pre-Research Foundation of China (No. 61403120207), the Aeronautical Science Foundation of China (No. 20185142003), Natural Science Foundation of Henan Province, China (No. 222300420433), the Science and Technology Innovative Talents in Universities of Henan Province (No. 21HASTIT030), Young Backbone Teachers in Universities of Henan Province (No. 2020GGJS073).

Conflicts of Interest: The authors declare no conflict of interest.

References

1. Fiscante, N.; Addabbo, P.; Clemente, C.; Biondi, F.; Giunta, G.; Orlando, D. A track-before-detect strategy based on sparse data processing for air surveillance radar applications. *Remote Sens.* **2021**, *13*, 662. [CrossRef]
2. Sun, L.; Yu, H.; Lan, J.; Fu, Z.; He, Z.; Pu, J. Tracking of Multiple Maneuvering Random Hypersurface Extended Objects Using High Resolution Sensors. *Remote Sens.* **2021**, *13*, 2963. [CrossRef]
3. Sun, L.; Zhang, J.; Yu, H.; Fu, Z.; He, Z. Tracking of Maneuvering Extended Target Using Modified Variable Structure Multiple-Model Based on Adaptive Grid Best Model Augmentation. *Remote Sens.* **2022**, *14*, 1613. [CrossRef]
4. Yang, S.; Baum, M. Tracking the orientation and axes lengths of an elliptical extended object. *IEEE Trans. Signal Process.* **2019**, *67*, 4720–4729. [CrossRef]
5. Lan, J.; Li, X.R. Extended-object or group-target tracking using random matrix with nonlinear measurements. *IEEE Trans. Signal Process.* **2019**, *67*, 5130–5142. [CrossRef]
6. Zhang, L.; Lan, J. Tracking of extended object using random matrix with non-uniformly distributed measurements. *IEEE Trans. Signal Process.* **2021**, *69*, 3812–3825. [CrossRef]
7. Feldmann, M.; Fränken, D.; Koch, W. Tracking of extended objects and group targets using random matrices. *IEEE Trans. Signal Process.* **2010**, *59*, 1409–1420. [CrossRef]
8. Granstrom, K.; Baum, M.; Reuter, S. Extended object tracking: Introduction, overview and applications. *J. Adv. Inf. Fusion* **2017**, *12*, 139–174.
9. Zea, A.; Faion, F.; Baum, M.; Hanebeck, U.D. Level-set random hypersurface models for tracking nonconvex extended objects. *IEEE Trans. Aerosp. Electron. Syst.* **2016**, *52*, 2990–3007. [CrossRef]
10. García-Fernández, Á.F.; Svensson, L.; Morelande, M.R. Multiple target tracking based on sets of trajectories. *IEEE Trans. Aerosp. Electron. Syst.* **2019**, *56*, 1685–1707. [CrossRef]
11. Beard, M.; Reuter, S.; Granström, K.; Vo, B.T.; Vo, B.N.; Scheel, A. Multiple extended target tracking with labeled random finite sets. *IEEE Trans. Signal Process.* **2015**, *64*, 1638–1653. [CrossRef]
12. Siew, P.M.; Linares, R.; Bageshwar, V.L. Extended target tracking and shape estimation via random finite sets. In Proceedings of the 2019 American Control Conference (ACC), Philadelphia, PA, USA, 10–12 July 2019; pp. 5346–5351.
13. Koch, J.W. Bayesian approach to extended object and cluster tracking using random matrices. *IEEE Trans. Aerosp. Electron. Syst.* **2008**, *44*, 1042–1059. [CrossRef]

14. Granstrom, K.; Lundquist, C.; Orguner, U. Tracking rectangular and elliptical extended targets using laser measurements. In Proceedings of the 14th International Conference on Information Fusion, Chicago, IL, USA, 5–8 July 2011.
15. Lan, J.; Li, X.R. Tracking of maneuvering non-ellipsoidal extended object or target group using random matrix. *IEEE Trans. Signal Process.* **2014**, *62*, 2450–2463. [CrossRef]
16. Baum, M.; Hanebeck, U.D. Shape tracking of extended objects and group targets with star-convex RHMs. In Proceedings of the 14th International Conference on Information Fusion, Chicago, IL, USA, 5–8 July 2011; pp. 1–8.
17. Baum, M.; Hanebeck, U.D. Extended Object Tracking with Random Hypersurface Models. *IEEE Trans. Aerosp. Electron. Syst.* **2014**, *50*, 149–159. [CrossRef]
18. Baum, M. Simultaneous Tracking and Shape Estimation of Extended Objects. Ph.D. Thesis, Karlsruhe Institute of Technology (KIT), ISAS—Intelligent Sensor-Actuator-Systems Laboratory, Karlsruhe, Germany, 2013.
19. Sun, L.; Lan, J.; Li, X.R. Extended target tracking using star-convex model with nonlinear inequality constraints. In Proceedings of the 31st Chinese Control Conference, Hefei, China, 25–27 July 2012; pp. 3869–3874.
20. Li, X.R.; Jilkov, V.P. Survey of maneuvering target tracking. Part I. Dynamic models. *IEEE Trans. Aerosp. Electron. Syst.* **2003**, *39*, 1333–1364.
21. Chen, H.; Du, J. An adaptive contour algorithm for irregular shape extended target. In Proceedings of the 2017 IEEE International Conference on Mechatronics and Automation (ICMA), Kagawa, Japan, 6–8 August 2017; pp. 734–739.
22. Sun, L.; Yu, H.; Fu, Z.; He, Z.; Zou, J. Modeling and Tracking of Maneuvering Extended Object With Random Hypersurface. *IEEE Sensors J.* **2021**, *21*, 20552–20562. [CrossRef]
23. Li, X.R.; Bar-Shalom, Y. Design of an interacting multiple model algorithm for air traffic control tracking. *IEEE Trans. Control. Syst. Technol.* **1993**, *1*, 186–194. [CrossRef]
24. Sun, L.; Zhang, S.; Ji, B.; Pu, J. Performance evaluation for shape estimation of extended objects using a modified hausdorff distance. In Proceedings of the 2016 IEEE International Conference on Information and Automation (ICIA), Ningbo, China, 1–3 August 2016; pp. 780–784.
25. Jin, F.; Pei, L.; Chen, H.; Zhou, L. Interval-valued intuitionistic fuzzy continuous weighted entropy and its application to multi-criteria fuzzy group decision making. *Knowl.-Based Syst.* **2014**, *59*, 132–141. [CrossRef]
26. Jin, F.; Ni, Z.; Chen, H.; Li, Y.; Zhou, L. Multiple attribute group decision making based on interval-valued hesitant fuzzy information measures. *Comput. Ind. Eng.* **2016**, *101*, 103–115. [CrossRef]
27. Mühlenbein, H.; Höns, R. The estimation of distributions and the minimum relative entropy principle. *Evol. Comput.* **2005**, *13*, 1–27. [CrossRef]
28. Adams, T. Continuous, Full-scope, Spatio-temporal Tracking Metric based on KL-divergence. In Proceedings of the 2019 IEEE Winter Applications of Computer Vision Workshops (WACVW), Waikoloa Village, HI, USA, 7–11 January 2019; pp. 16–24.
29. Gour, G.; Tomamichel, M. Entropy and relative entropy from information-theoretic principles. *IEEE Trans. Inf. Theory* **2021**, *67*, 6313–6327. [CrossRef]
30. Liao, H.; Xu, Z. Approaches to manage hesitant fuzzy linguistic information based on the cosine distance and similarity measures for HFLTSs and their application in qualitative decision making. *Expert Syst. Appl.* **2015**, *42*, 5328–5336. [CrossRef]
31. Lin, Y.; Wang, Y.M.; Yan, L. Cosine-similarity based approach for weights determination under hesitant fuzzy environment and its extension to priority derivation. *J. Intell. Fuzzy Syst.* **2020**, *38*, 2261–2271. [CrossRef]